Chinese Journal of Chemical Engineering 90 (2026) 283–292

Contents lists available at ScienceDirect

Chinese Journal of Chemical Engineering

journal homepage: www.elsevier.com/locate/CJChE

Full Length Article

Fabrication of composite microspheres doped with nano-aluminum powder using melt spray technology

Yilin Liu [1], Lanqi Zhang [2], Yulong Yin [2], Nan Li [3], Xiangnan Chu [4], Qi Ma [4], Jing Liu [1], Wenbo Yang [1,*], Yingdi Lv [5,6,*], Shengyang Tao [1,*]

[1] School of Chemistry, State Key Laboratory of Fine Chemicals, Frontier Science Center for Smart Materials, Dalian Key Laboratory of Intelligent Chemistry, Dalian University of Technology, Dalian 116024, China
[2] China Nuclear Power Operations Co., Ltd., Shenzhen 518000, China
[3] Suzhou Nuclear Power Research Institute Co., Ltd., Suzhou 215004, China
[4] Yangjiang Nuclear Power Co., Ltd., Yangjiang 529941, China
[5] School of Chemistry and Chemical Engineering, Northwestern Polytechnical University, Xi'an 710129, China
[6] Xi'an Modern Chemistry Research Institute, Xi'an 710065, China

ARTICLE INFO

Article history:
Received 26 July 2025
Received in revised form
21 September 2025
Accepted 22 September 2025
Available online 17 October 2025

Keywords:
Melt spray
Micro-nano composite material
Amorphous structure
Composite microspheres

ABSTRACT

Melt spray technology serves as an effective method for fabricating spherical micro-nano composite materials, with established applications in catalysts and pharmaceuticals. This study extends its application to energetic composite microspheres, investigating the microsphere formation process using nano-aluminum powder (nano-Al) combined with the inert surrogate sucrose octaacetate (SOA). This study systematically investigates the effects of process parameters, formulation composition, and storage conditions on the particle size, morphology, and stability of SOA/Al composite microspheres. Higher atomizing gas pressure and temperature significantly reduced median particle diameter (D_{50}), yielding a D_{50} of 35.09 μm at 150 °C and 200 kPa. The addition of polyethylene glycol: polyvinylpyrrolidone (1:1) enhanced microsphere circularity from 0.67 to 0.85. This system produced 78 g composite microspheres within 20 min, demonstrating efficient lab-scale production. X-ray diffraction and differential scanning calorimetry results indicated that rapid cooling led to amorphous structures, which were stabilized during storage at 4 °C. The scalable melt spray fabrication strategy developed here for nanoparticle-doped composite microspheres provides a basis for future studies involving diverse functional composites.

1. Introduction

Microparticles and nanoparticles exhibit substantial application potential in fields [1] such as pharmaceuticals [2,3], energy storage [4], coatings [5], and energetic materials [6]. Micro-nano composite materials not only mitigate the aggregation tendencies of single component nanoparticles but also preserve the unique surface characteristics and functionalities of the constituent particles. Spherical micro-nano composite materials exhibit a higher specific surface area and enhanced flowability relative to other morphologies. Furthermore, they allow for greater control over particle size and shape uniformity, critical for stable material performance. Common preparation methods for composite microspheres include spray drying [7–9], self-assembly [10,11], templating [12], microemulsion [13], droplet microfluidics [14], and melt spray technology [15]. Spray drying requires solvent evaporation, leading to residual solvent issues and high energy consumption. Self-assembly, templating, and microemulsion methods involve complex processes, low microsphere formation efficiency, and demanding post-processing steps. Microfluidic systems face clogging risks due to small channel sizes, cannot handle high-viscosity liquids, and remain costly with limited production capacity [16]. Among these methods, melt spray technology effectively combines hot-melt extrusion and spray drying for producing composite microspheres. Molten materials doped with functional powders are subjected to atomizing gas pressure in the atomizer, leading to the formation of fine droplets *via* complex droplet breakup. These droplets rapidly solidify in a cooling medium, ultimately yielding micron-scale particles. This

* Corresponding authors.
E-mail addresses: wbyang@dlut.edu.cn (W. Yang), imlv1984@126.com (Y. Lv), taosy@dlut.edu.cn (S. Tao).

https://doi.org/10.1016/j.cjche.2025.09.014
1004-9541/

method offers operational simplicity, high-throughput production potential, and tunable particle sizes. Without solvent evaporation, the composite microspheres exhibit dense, solid-core structures and can be collected as free-flowing powder without complex post-processing compare to other methods. For example, in biocatalysis, melt spray technology enables effective enzyme immobilization by atomizing molten carrier-enzyme mixtures [17]. In pharmaceutical preparation, semi-crystalline solid dispersions produced *via* this method efficiently deliver poorly water-soluble active pharmaceutical ingredients (APIs) [18]. In nuclear materials, melt spray technology is used to prepare Li_4SiO_4 ceramic microspheres for tritium breeding, which meet the requirements of fusion reactors for high density and thermal stability [19].

Aluminum powder is commonly introduced as a high-energy metal fuel due to its high combustion enthalpy and density [20]. To enhance the overall performance of energetic systems and mitigate the agglomeration of nano-aluminum powder (nano-Al) during combustion [21], researchers commonly synthesize composite microspheres by integrating nano-Al with high-energy oxidizers [22,23]. Futhermore, energetic composite microspheres doped with nano-Al feature high energy density, excellent combustion behavior, high bulk density, and low sensitivity for safer processing and transportation [24–26]. However, current fabrication methods still encounter challenges such as poor control over particle size and morphology, as well as limited scalability for industrial production. Melt spray technology, by contrast, offers significant advantages that align well with the design requirements of energetic composite microspheres doped with nano-Al, including high efficiency, low cost, controllable particle morphology, and suitability for continuous, large-scale manufacturing. Therefore, applying melt spray technology to the preparation of energetic materials is both technically feasible and promising for further investigation.

However, conducting melt spray experiments directly using highly reactive and sensitive energetic oxidizers combined with nano-Al is challenging, due to factors such as high material costs, substantial manpower requirements, and significant safety risks. Therefore, this study employs a composite system of inert substitute material and nano-Al as a model system, aiming to investigate the effects of key process parameters on the microsphere under safer and more cost-effective conditions. Sucrose octaacetate (SOA) was selected as an inert substitute material (Table S1 in Supplementary Material presents similar properties of partial high-energy oxidizers and SOA [27–30]). This strategy provides a controllable and safe platform for simulating the composite formation and shaping processes of energetic materials doped with nano-Al. Based on this system, SOA/Al composite microspheres were successfully prepared *via* melt spray technology. The effects of processing parameters and formulation design on the microsphere characteristics were systematically investigated, and the impact of post-treatment methods on their physical stability was evaluated. This study not only reveals critical control factors for the melt spray preparation of such composite materials, but also provides fundamental data and process references for future applications in energetic systems.

2. Experimental

2.1. Materials and experimental equipment

Nano-aluminum powder (nano-Al) was supplied by Xi'an Modern Chemistry Research Institute, China. Sucrose octaacetate (SOA) was obtained from Macklin Biochemical Co., Ltd., Shanghai, China. Methanol (analytical grade) was supplied by Kemiou Chemical Reagent Co., Ltd., Tianjin, China. Polyethylene glycol (PEG, $M_W = 4000$) and polyvinylpyrrolidone (PVP K30) were obtained from Guangfu Fine Chemical Research Institute, Tianjin, China. Poly (ethylene glycol)-block-poly (propylene glycol)-block-poly (ethylene glycol) (P123) was obtained from Sigma-Aldrich (Shanghai) Trading Co., Ltd, China. Hydroxypropylmethylcellulose (HPMC) was purchased from Macklin Biochemical Co., Ltd., Shanghai, China.

The digital display constant-temperature heating magnetic stirrer (MS7-H550/H280/380-Pro) was purchased from Beijing Dalong Xingchuang Experimental Instrument Co., Ltd., China. The high-pressure air compressor (BDZ7031/1.5) was purchased from Beijing Oupuke Compression Equipment Co., Ltd., China. The microfluidic pressure pump (OB1 MK3+) was purchased from ElveFlow, France. The annular heating jacket was purchased from Jiangyin Huachen Qidian Electric Appliance Co., Ltd., Wuxi, China. The solid-state relay (four-channel) was purchased from Anthone Electric Co., Ltd., Xiamen, China. The temperature sensor (PT100) and the heating rod (Pt) was purchased from Beijing Huasheng Shida Technology Co., Ltd., China.

2.2. Preparation setup

A melt spray system for preparing composite microspheres was constructed in this study, as illustrated in Fig. 1. The setup comprises a microfluidic pressure pump (ElveFlow), a high-pressure air compressor, a stainless-steel syringe, an annular heating jacket, a nozzle thermostat, a triple-channel internal-mixing

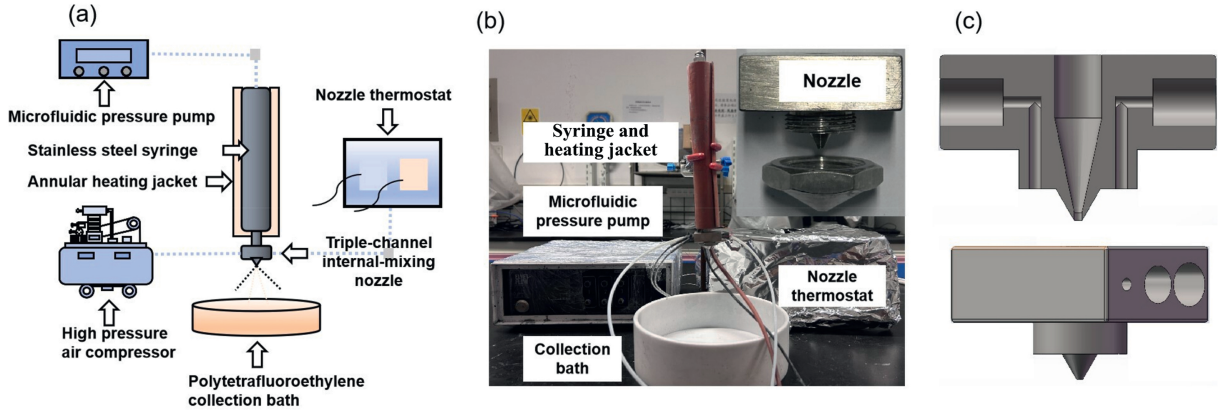

Fig. 1. (a) Schematic diagram of the composite microsphere preparation setup; (b) Photographic illustration of the experimental apparatus; (c) Cross-sectional schematic of the nozzle structure.

nozzle, and a polytetrafluoroethylene (PTFE) collection vessel (Fig. 1(a), (b)). The system delivers the liquid *via* pressure injection controlled by the microfluidic pressure pump, while the atomizing gas pressure is regulated by the high-pressure air compressor. The pre-mixed molten material is loaded into a gas-assisted stainless-steel syringe (Japanese-style luer-lock design) with excellent thermal conductivity, serving as the feed reservoir. The annular heating jacket heats and maintains the temperature of the stainless-steel syringe, with a temperature range up to 200 °C. The nozzle thermostat employs a 50 W heating rod and a PT100 temperature sensor, utilizing a PID temperature control algorithm managed by a four-channel solid-state relay. The parameter of the temperature control system and the annular heating jacket can be found in Table S2. A cross-sectional schematic and photograph of the triple-channel internal-mixing nozzle is illustrated in Fig. 1(b), (c). The central channel transports the molten material and the compressed air was ejected symmetrically from two gas outlets. This high-velocity airflow sheared the liquid stream and broke it into fine droplets at the nozzle exit. Three lateral ports (Fig. 1(c)) are connected to the temperature sensor, high-velocity airflow inlet tube, and the Pt heating rod from left to right. Fig. S1 and Table S3 provide further details about the nozzle. The PTFE collection vessel exhibits stable chemical properties, ensuring no reaction with system components. The selection of the receiving bath medium can be found in Fig. S2.

2.3. Preparation process

The composite microspheres were prepared through a three-stage process comprising melting, atomization, and solidification. The preparation of a precursor solution containing 20% (mass) nano-Al and 80% (mass) SOA involves the following steps. First, 6 g of nano-Al and 24 g of SOA were added to a beaker containing 15 ml of methanol as the solvent. The mixture was initially heated to 30 °C to allow dissolution. After this, the temperature was increased stepwise by 10 °C increments (with each step held for 5 min) until it reached 60 °C. Once stabilized at 60 °C, the system was then maintained at 60 °C for 30 min until complete solvent evaporation. Subsequently, the temperature was raised to 150 °C, and the mixture was stirred for 3 h under 400 $r \cdot min^{-1}$ to ensure homogeneity. At this point, the material was melted and loaded into a preheated stainless-steel syringe. Subsequently, the molten liquid was delivered through the nozzle at 50 kPa using a microfluidic pressure controller, while the high-velocity airflow generated by the air compressor induced fragmentation of droplets at the nozzle outlet. The resulting droplets were then immediately quenched in a liquid nitrogen PTFE collection vessel to achieve rapid solidification. Following complete evaporation of the liquid nitrogen, the solidified microspheres were harvested and preserved at 4 °C for subsequent characterization and application.

2.4. Analytical characterization

The surface morphology, elemental distribution, and the particle size of the composite microspheres were characterized by field-emission scanning electron microscope (FE-SEM, Nova NanoSEM 450, FEI, USA), equipped with an energy-dispersive X-ray spectroscopy (EDS) detector. Prior to imaging, the samples were mounted on conductive adhesive tapes and sputter-coated with a 10 nm platinum layer to enhance surface conductivity. EDS elemental mapping was performed on both the surface and cross-sections areas of the microspheres to analyze the spatial distribution of aluminum, with an acquisition time of 60 s. The particle size of the microspheres was also characterized by using an inverted fluorescence microscope (Eclipse Ti2-U, Nikon, Japan). The aluminum content in the composite was quantitatively analyzed by thermogravimetric analysis (TGA) using a Q500 (TA Instruments, USA). Approximately 3.32 mg of the sample was placed in an open platinum crucible and heated from ambient temperature to 800 °C under an air atmosphere. The thermal behavior of the SOA was analyzed *via* differential scanning calorimetry (DSC 300, NETZSCH, Germany). Approximately 5.39 mg of sample was sealed in a standard aluminum crucible, with an empty crucible used as a reference. The measurement was conducted under nitrogen atmosphere (20 $ml \cdot min^{-1}$) following a thermal protocol consisting of heating from 25°C to 160 °C at 10 $°C \cdot min^{-1}$, cooling to 5 °C, and reheating to 160 °C at the same rate. The crystalline structure of the samples was characterized by X-ray diffraction (XRD, SmartLab 9 kW, Rigaku, Japan) with Cu K_α radiation. The powdered samples were evenly spread onto quartz sample holders. Data were collected over a 2θ range of 5°–80° at a scanning rate of 20 $(°) \cdot min^{-1}$. The size distribution and morphological parameters of the microspheres were analyzed based on ImageJ software. The circularity (C) was calculated according to Eq. (1),

$$C = \frac{4\pi A}{L^2} \tag{1}$$

where A represents the two-dimensional projection area of the microsphere and L denotes its perimeter.

3. Results and Discussion

3.1. Process parameter optimization and morphology control of composite microspheres

In the field of energetic materials, a higher content of nano-Al, as a high-energy metal fuel, typically enhances both the energy density and combustion performance [31]. To determine the optimal Al doping level for subsequent experiments, precursor solutions with Al mass contents of 10%, 20%, 30%, and 40% were prepared for spray experiments. When the nano-Al doping levels reached 30% and 40%, nozzle clogging occurred. This phenomenon can be attributed to the reduced fluidity of the molten materials, which is caused by the uneven dispersion of solid particles in high solid-loading systems, ultimately leading to flow instability and nozzle blockage. To demonstrate the process advantages of the melt spray system in atomizing high solid-loading formulations, the nano-Al doping level was set at 20% (mass). Fig. S3 demonstrates the SEM images of the nano-Al in this study.

In the melt spray process, molten material with excessive viscosity not only hinders effective jetting through the nozzle but also causes uneven atomization, which compromises product quality and performance, potentially leading to equipment clogging or failure. Therefore, the viscosity of the molten material must be maintained within a specific range to ensure smooth processing (Fig. 2). To optimize this process, the viscosity–temperature curve of the molten component SOA was measured (Fig. 2(a)). The viscosity of SOA exhibited distinct nonlinear behavior as the temperature increased. Initially, with a gradual rise in temperature, the viscosity decreased rapidly, indicating that the fluidity of the molten material was significantly affected by temperature in the lower range. When the temperature exceeded 120 °C, the viscosity continued to decrease, yet at a significantly reduced rate. Experiments demonstrated that nozzle clogging was largely prevented when the temperature reached 120 °C or higher. However, excessively high temperatures may induce thermal decomposition of raw materials, shorten the lifespan of equipment, and increase energy consumption during atomization. As a result, the effects of

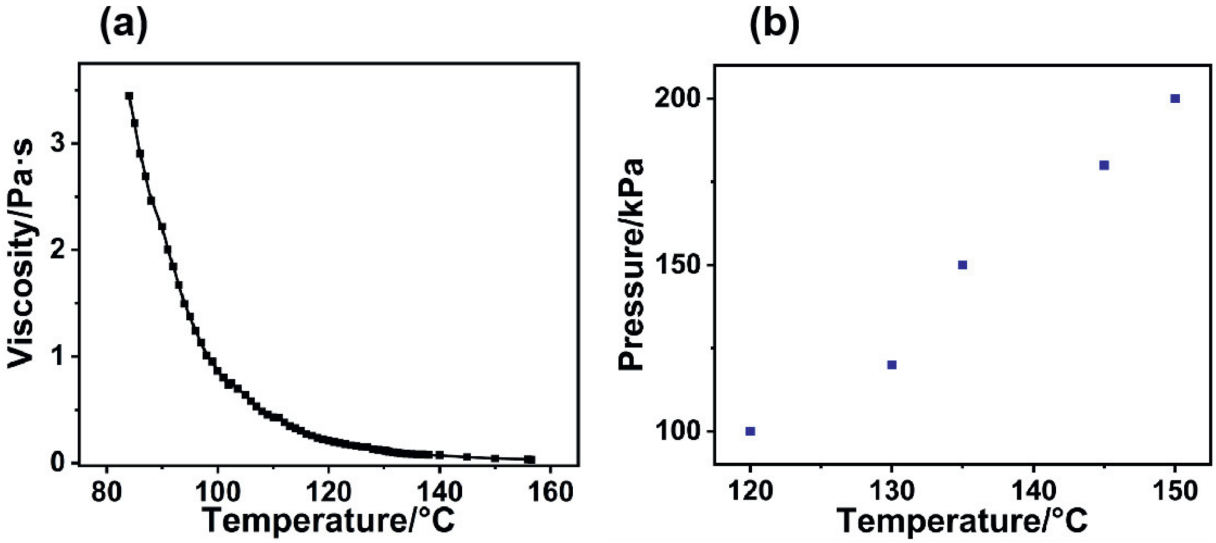

Fig. 2. (a) Viscosity–temperature curve of SOA. (b) Relationship between maximum atomizing gas pressure and temperature.

process parameters on microsphere morphology were investigated within the temperature range of 120°C–150 °C.

The shear force exerted by high-pressure gas on the molten liquid is of paramount importance for atomization. Excessive atomizing gas pressure hinders liquid ejection from the nozzle and may even induce backflow. Insufficient atomizing gas pressure is unable to supply sufficient energy for atomization, thereby leading to an extremely low atomization efficiency. Based on experimental results, the maximum atomizing gas pressure corresponding to various temperatures was investigated, as shown in Fig. 2(b). Within the temperature range of 120°C–150 °C, the adjustable maximum gas pressure increased from 100 to 200 kPa. When the delivery pressure was maintained at 50 kPa, a decrease in temperature led to a significant increase in the viscosity of the molten liquid. According to the Poiseuille Eq. (2) [32], under near-constant flow conditions, the pressure drop (ΔP) is proportional to the liquid viscosity (η). As the viscosity increases, the flow resistance of the molten feed within the stainless-steel barrel also increases, leading to a larger pressure drop from the top to the bottom. When the driving pressure is maintained at 50 kPa, this

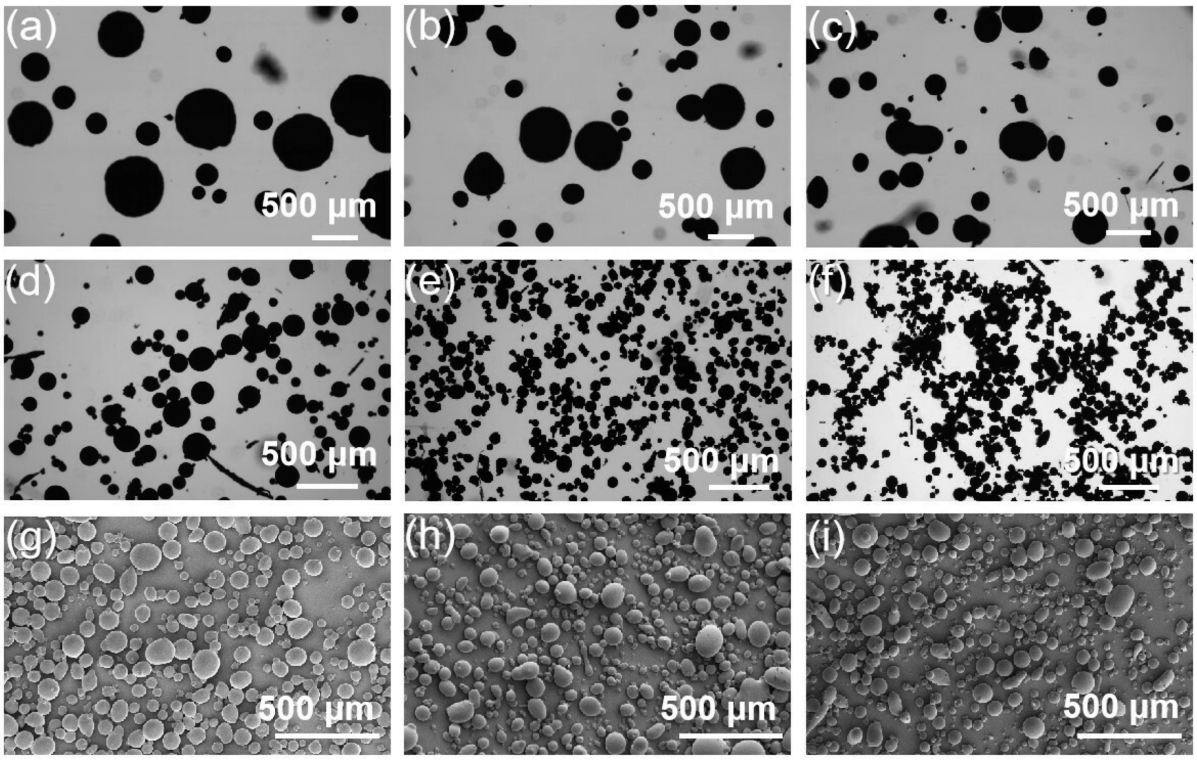

Fig. 3. Representative optical microscopy and SEM images of composite microspheres: (a) 120 °C (50 kPa), (b) 135 °C (50 kPa), (c) 150 °C (50 kPa), (d) 120 °C (100 kPa), (e) 135 °C (100 kPa), (f) 150 °C (100 kPa), (g) 135 °C (150 kPa), (h) 150 °C (150 kPa), (i) 150 °C (200 kPa).

pressure loss reduces the effective driving force at the nozzle outlet. In this case, the molten material cannot overcome the radial component of the atomizing gas due to the narrow nozzle outlet and insufficient driving force. As a result, atomization cannot proceed. In contrast, low-viscosity melts experience lower flow resistance and smaller pressure drops. Thus, a higher effective force is retained at the nozzle outlet, allowing the melt to overcome the radial gas flow and maintain continuous atomization.

$$\Delta P = \frac{8\eta LQ}{\pi r^4} \tag{2}$$

where ΔP represents the pressure drop, η is the viscosity of the fluid, L is the length of the pipeline, Q is the volumetric flow rate, and r is the radius of the pipeline.

To investigate the effects of the temperature and the atomizing gas pressure on the particle size of composite microspheres, the microspheres were prepared at temperatures of 120, 135, and 150 °C under spray pressures of 50, 100, 150, and 200 kPa. Fig. 3 displays the representative images of composite microspheres under various experimental conditions. Characterization methods were selected by different size range. Specifically, optical microscopy for statistical of large particles (Fig. 3(a)–(f)), SEM for resolution of small particles (Fig. 3(g)–(i)). Fig. 4 illustrates the particle size distribution histograms.

Table 1
The particle size of composite microspheres under different conditions ①.

Entry	Temperature/°C	Pressure/kPa	D_{50}②/μm
1	120	50	248.90
2	120	100	89.29
3	135	50	218.03
4	135	100	71.77
5	135	150	56.78
6	150	50	213.81
7	150	100	68.75
8	150	150	44.75
9	150	200	35.09

① The particle size span illustrates in Table S4.
② D_{50} represents the median size of particles.

The particle sizes of the composite microspheres and the corresponding experimental conditions are summarized in Table 1. At 150 °C, under spray pressures of 50, 100, 150, and 200 kPa, the median particle sizes of the composite microspheres were 213.81, 68.75, 44.75, and 35.09 μm, respectively. At 135 °C, under spray pressures of 50, 100, and 150 kPa, the median particle sizes were 218.03, 71.77, and 56.78 μm, respectively. The results demonstrate that, at constant temperature, higher gas pressures result in smaller average particle sizes of the composite microspheres. When the atomization pressure decreased from 100 to 50 kPa, the particle sizes of composite microspheres under all temperature conditions sharply increased to more than

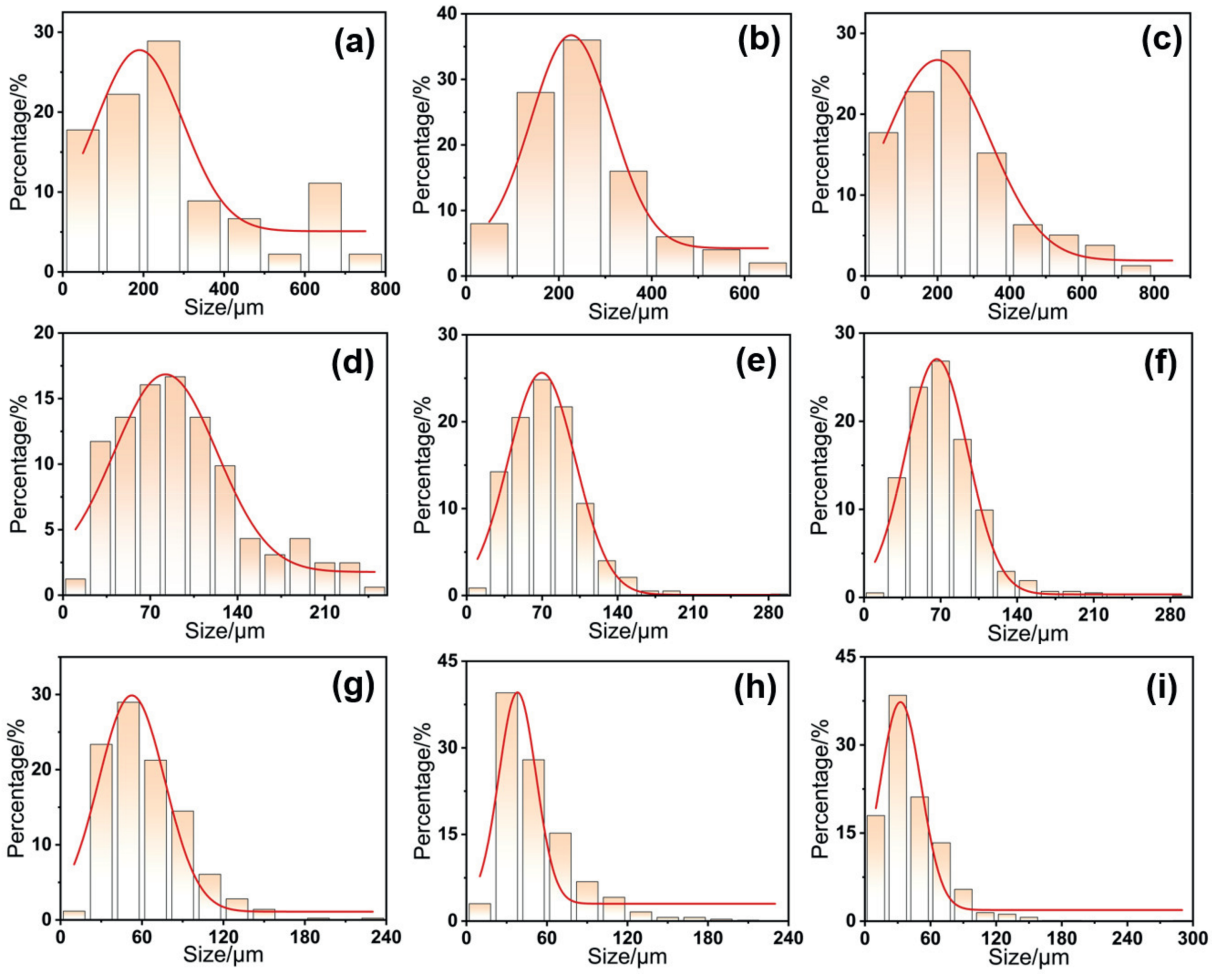

Fig. 4. Particle size distribution histograms of composite microspheres prepared under different process parameters: (a) 120 °C (50 kPa), (b) 135 °C (50 kPa), (c) 150 °C (50 kPa), (d) 120 °C (100 kPa), (e) 135 °C (100 kPa), (f) 150 °C (100 kPa), (g) 135 °C (150 kPa), (h) 150 °C (150 kPa), (i) 150 °C (200 kPa).

200 μm, which indicates an extremely low atomization efficiency at 50 kPa.

As described in Eq. (2) [33], the particle size is inversely proportional to the gas–liquid relative velocity and directly proportional to viscosity and surface tension of the liquid. From the perspective of the atomization mechanisms, the triple-channel internal-mixing nozzle employed in this study conveys the molten material through the central tube, and compressed air escapes through two gas outlets in the annular gap. When gas–liquid two-phase flows interact at the outlet of the nozzle, the airflow and liquid flow display three distinct breakup modes, namely droplet breakup, ligament breakup, and film breakup, which are dependent on their relative velocities. Among these breakup modes, the film breakup mode fragments the liquid into fine droplets. Initially, high-speed airflow stretches the liquid into a thin film, and this thin film subsequently experiences secondary breakup to form micron-sized droplets [34]. Increasing gas pressure significantly enhances the shear intensity and kinetic energy of the gas flow at the nozzle. Therefore, when the gas flow interacts with the molten feedstock, the intensified shear forces stretch the liquid film into thinner layers and accelerate the fragmentation process (primary atomization). Simultaneously, the turbulent kinetic energy of the high-speed gas flow triggers secondary droplet breakup (secondary atomization), resulting in smaller droplet sizes. In this process, more kinetic energy is converted into the surface energy of droplets. However, it should be noted that when the droplet size becomes sufficiently small, surface tension dominates and prevents further breakup.

$$D = 585\frac{\sqrt{\sigma_L}}{v\sqrt{\rho_L}} + 597\left(\frac{\mu_L}{\sqrt{\sigma_L\rho_L}}\right)^{0.45}\left(1000\frac{Q_L}{Q_a}\right)^{1.5} \quad (3)$$

In Eq. (3), D represents the droplet diameter. ρ_L denotes the liquid density. σ_L is the liquid surface tension. μ_L refers to the liquid viscosity. v corresponds to the relative velocity between the gas and liquid. Q_L indicates the liquid volumetric flow rate, and Q_a is the air volumetric flow rate.

Under spray temperatures of 120, 135, and 150 °C, the composite microspheres prepared at an atomizing gas pressure of 100 kPa exhibited median diameters of 89.29, 71.77, and 68.75 μm, respectively. As the spray temperature increased from 120°C to 150 °C, the viscosity of the molten material decreased from 0.21 to 0.04 Pa·s. Experimental results indicate that, when the shear force magnitude and nanoparticle doping level remain constant, the average particle size of the composite microspheres decreases with the increasing of temperature. As shown in Eq. (3), the average particle size is proportional to the liquid viscosity. This mechanism can be attributed to the inhibitory effect of viscous resistance on the droplet breakup process. When the viscosity increases, the internal friction between molecules in the melt becomes stronger, which weakens the stretching and breakup effects of shear forces on the liquid film. As a result, more energy is dissipated to overcome internal friction rather than being converted into surface energy for droplet fragmentation, leading to the formation of larger droplets. Conversely, when viscosity decreases, improved melt fluidity allows shear energy to be efficiently converted into droplet surface energy, promoting liquid film destabilization and the generation of smaller micron-sized droplets.

To evaluate the incorporation of nano-Al in the composite microspheres prepared *via* melt spray technology, EDS analysis was conducted on both the surface and cross-sections of microspheres synthesized at 150 °C and 200 kPa. The EDS results (Fig. 5) indicate that Al elemental signals (purple regions) are present in both regions, confirming successful doping of nano-Al throughout the microspheres. EDS of composite microspheres prepared under different processing conditions are shown in Fig. S4 and Fig. 5. TGA was performed on the composite microspheres prepared at 150 °C and 200 kPa. Fig. 5(e) shows the TGA curves of the composite microspheres and SOA. The results illustrate that the weight of the composite microspheres decreased markedly upon heating to 200 °C, indicating the onset of thermal decomposition of the components. As the temperature approached 340 °C, the weight stabilized. The residual mass of the composite microspheres was 21%, compared to approximately 1% for SOA at the same temperature. This difference (20%) is consistent with the 20% content of nano-Al in the original formulation. Furthermore, beyond 550 °C, the weight of the composite sample increased, which is attributed to oxidation of nano-Al in the oxygen-containing atmosphere.

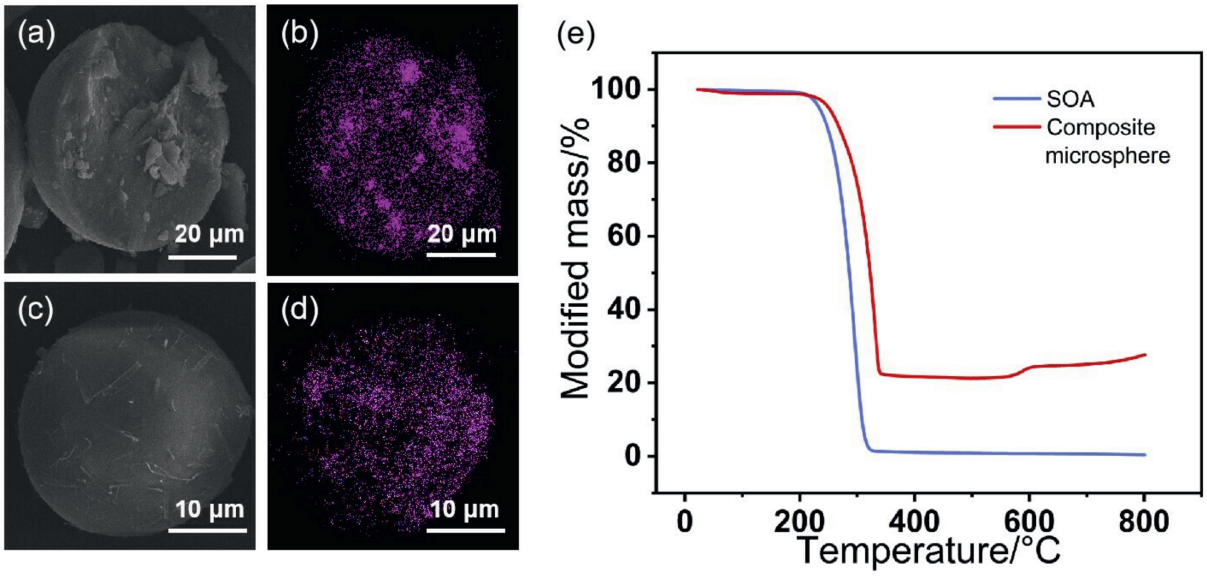

Fig. 5. (a)–(d) EDS of Al element of composite microsphere under 200 kPa, 150 °C, and 400 r·min^{-1}. (e) Thermogravimetric analysis (TGA) curves of composite microsphere and SOA.

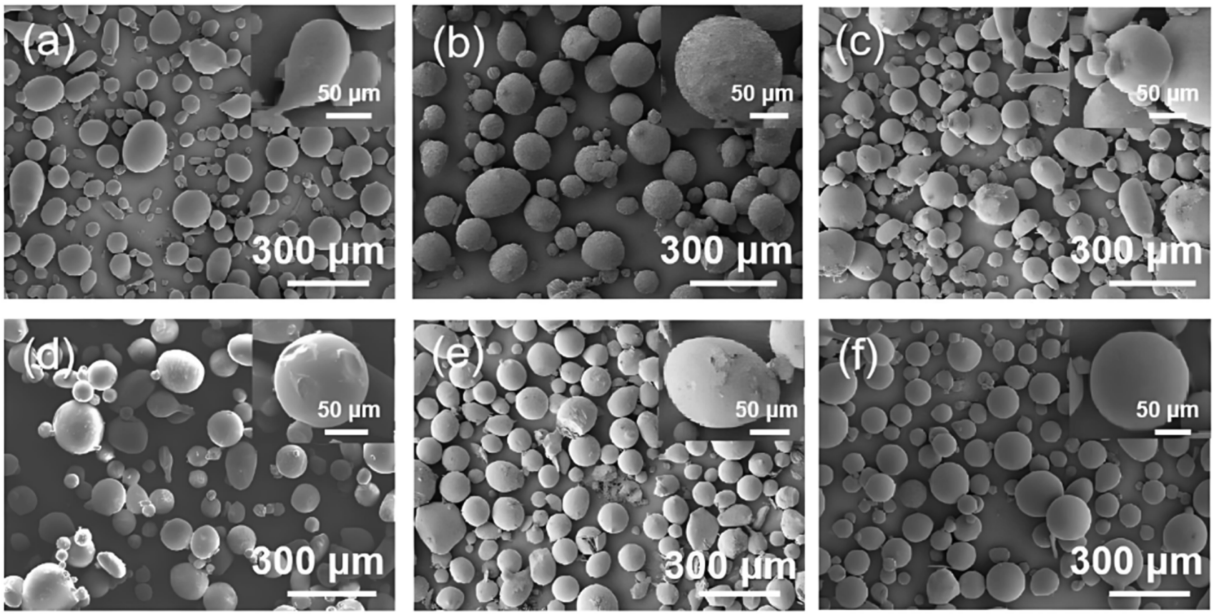

Fig. 6. SEM images of representative composite microspheres: (a) without polymer additives and (b)–(f) with 2.5% (mass) polymer additives. ((b) P123, (c) PEG:HPMC 1:1, (d) PEG, (e) PVP, (f) PEG:PVP 1:1)

3.2. Effect of additives on microspheres

Composite microspheres prepared using a molten material formulation containing 20% nano-Al and 80% SOA exhibited low average circularity (0.67) and filamentous structures (Fig. 6(a)). Various polymer additives (including PVP, PEG, HPMC, and P123) were introduced into the molten matrix for optimization. These selected polymer additives were thermally stable within the 120°C—150 °C. SEM images of microspheres with different additives (Fig. 6) were analyzed using ImageJ software. Table 2 shows the average circularity of composite microspheres under different conditions. As seen in the SEM images, after adding P123, the microsphere surface became rough with needle-like crystals. Particle agglomeration was observed, and the average circularity was 0.68 (Fig. 6(b)). With the PEG:HPMC (1:1) blended additive, rod-shaped and a few large irregular microspheres appeared. Some adhesion between particles was seen, and the average circularity was 0.70 (Fig. 6(c)). When the PEG additive was used solely, the microspheres had smoother surfaces, but slight adhesion was still present (Fig. 6(d)). The average circularity was 0.74. With the PVP additive, the surface was rough with wrinkles, but no adhesion between microspheres was observed. The average circularity was 0.77 (Fig. 6(e)). When the PEG:PVP (1:1) blended additive was added, the microspheres showed smooth surfaces with minimal deformation or adhesion. Furthermore, the average circularity of 0.85 was achieved (Fig. 6(f)).

Table 2
Average circularity of composite microspheres under different conditions [①].

Entry	Additives	$\overline{C}$ [③]	SD [④]
1	/ [②]	0.67	0.12
2	P123	0.68	0.09
3	PEG:HPMC 1:1	0.70	0.11
4	PEG	0.74	0.11
5	PVP	0.77	0.12
6	PEG:PVP 1:1	0.85	0.10

[①] Molten material formulation contains 20% (mass) nano-Al, 77.5% (mass) SOA, and 2.5% (mass) additives. The temperature is 150 °C and the atomization gas pressure is 100 kPa.
[②] There are only 20% (mass) nano-Al, and 80% (mass) SOA in this formula.
[③] $\overline{C}$ represents the arithmetic mean of circularity.
[④] SD represents the standard deviation.

The experimental results indicate that the synergistic effect of the PEG:PVP (1:1) blended additive simultaneously enhances the circularity and uniformity of the surface morphology of the composite microspheres. The melt spray process shares similar thermal processing principles with hot-melt extrusion (HME), permitting the application of polymer additive mechanisms derived from HME [35]. The improved performance may be attributed to the pseudoplastic behavior of both PVP and PEG, which is characterized by a decrease in viscosity with increasing shear stress. Under high shear forces and external driving pressures during the process, the rheological properties of the molten material are altered. This modification reduces the viscous resistance and the surface tension of the droplets, promoting rapid contraction into spherical structures *via* surface tension before solidification, thereby minimizing irregular particle formation and enhancing morphology uniformity and circularity. This conclusion provides a theoretical foundation for optimizing the melt spray technology through additive selection. After optimizing the circularity, this study further explored the advantages of production capacity in the melt spray technology. Experimental results indicate that this setup produced 78 g of composite microspheres within 20 min, demonstrating its potential for large-scale production. An outlook regarding the large-scale production potential is provided in the Supplementary Material.

3.3. Effects of cooling and storage conditions on composite microspheres

During room-temperature storage, irreversible deformation, characterized by initial softening followed by hardening and caking, was observed in the composite microspheres. SEM images of the microspheres upon storage, reveal an irregular overall morphology (Fig. 7). These changes suggest that structural

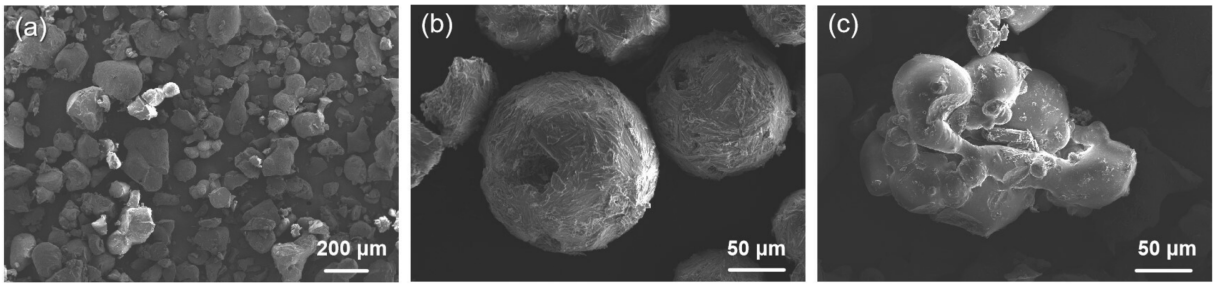

Fig. 7. SEM images of composite microspheres after hardening and caking: (a) morphology of most composite microspheres after caking, (b) composite microspheres that partially retain their spherical shape but exhibit surface pores and crystalline deposits, (c) composite microspheres with severely damaged morphology.

relaxation and interfacial fusion occurred during the storage period. To further elucidate the underlying mechanism, DSC and XRD analyses were conducted to investigate how the melt-cooling process influences the internal structure of the microspheres.

DSC analysis (Fig. 8) was employed to elucidate the thermal mechanisms underlying the hardening and caking behavior observed in SOA/Al composite microspheres. During the first heating cycle, SOA exhibited an endothermic peak between 80°C and 95 °C, indicative of crystalline phase melting. Upon cooling, a distinct stepwise decrease in heat flow was observed at approximately 25 °C, signifying the formation of a glassy state. This allowed the determination of the glass transition temperature (T_g) of SOA as 25 °C. During the second heating cycle, an endothermic peak near 25 °C was observed, corresponding to the softening of the amorphous glassy phase. No crystallization peaks were detected during either the initial cooling or subsequent heating cycle, which may be attributed to the experimental heating/cooling rates surpassing the critical crystallization threshold and thereby suppressing crystallization kinetics. The hardening and caking phenomena are associated with the molten material, which, after atomization and entry into the liquid nitrogen collection vessel, experiences rapid quenching. This rapid cooling prevents ordered crystallization, thereby trapping the composite microspheres in a supercooled liquid state [36]. When the system cools below the T_g, the viscosity increases sharply, significantly reducing molecular mobility and hindering structural rearrangement, resulting in a structure characterized by long-range disorder and short-range order. Conversely, storage near the T_g (25 °C) induces structural relaxation in the amorphous SOA, leading to

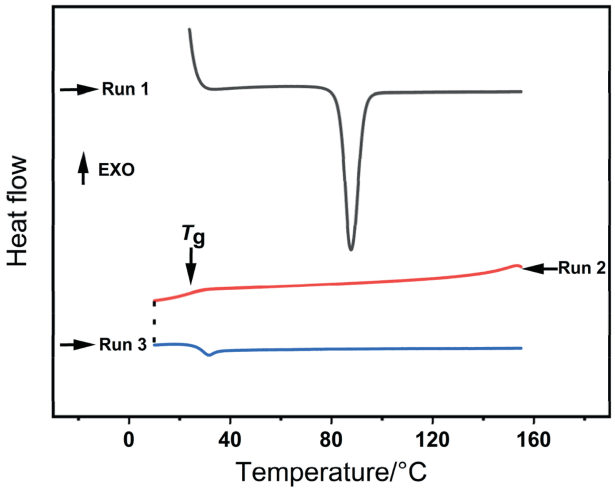

Fig. 8. DSC images of SOA.

internal flow, microsphere softening, and interparticle aggregation. Ultimately, this results in irreversible caking and the formation of densely agglomerated macroscopic structures.

To investigate the stability of the amorphous structure in composite microspheres, the crystallographic characteristics of SOA, nano-Al, and composite microspheres prepared at different preparation times were compared using XRD analysis (Fig. 9). The XRD pattern of SOA displayed distinct crystalline peaks in the 5°–40° range, which completely vanished in the composite microspheres, replaced by a broad amorphous halo near 20°, confirming the amorphous state of SOA. The characteristic diffraction peaks of nano-Al (38.5°, 44.7°, 65.1°, 78.2°) remained intact in the composite microspheres, verifying the successful doping of nano-Al without phase transformation.

XRD characterization of composite microspheres stored at different temperatures for one month (Fig. 9) demonstrated that the sample stored at room temperature (25 °C) displayed weak crystalline peaks within the 5°–40° range, coinciding with the crystalline peaks of SOA in Fig. 9(a). In contrast, the sample stored at 4 °C showed no SOA-related crystalline peaks, indicating that room temperature promotes the amorphous-to-crystalline transition. This phenomenon occurs because the amorphous state is thermodynamically metastable and tends to spontaneously evolve toward a lower-energy, more stable crystalline state [37]. The amorphous-crystalline transition can be explained by classical nucleation-growth theory, where the amorphous system undergoes two temperature-driven phase transformations comprising nucleation (Eq. (4)) and crystal growth (Eq. (5)) [38,39]. For the nucleation rate (J), molecular thermal motion is insufficient to overcome the energy barrier for forming critical nuclei at low temperatures (4 °C). The extremely low nucleation rate prevents the amorphous-to-crystalline transition. When the temperature approaches T_g, the thermodynamic driving force increases, significantly enhancing J. Regarding the growth rate (U), as the temperature rises from 4°C to 25 °C, viscosity decreases and molecular mobility increases, leading to a marked rise in U.

The classical homogeneous nucleation rate equation is expressed as follows,

$$J = A\exp\left(\frac{-16\pi\gamma^3}{3kT\cdot\Delta H_f^2 T_r(\Delta T_r)^2} - \frac{\Delta G'}{kT}\right) \tag{4}$$

where J represents the steady-state nucleation rate, A is a temperature-independent vibrational factor, γ is the interfacial tension between the crystalline surface and the medium, k is the Boltzmann constant, T is the measured temperature, ΔH_f is the enthalpy of melting, $T_r = T/T_m$ (T_m is the melting point), $\Delta T_r = \Delta T/T_m$ ($\Delta T = T_m - T$, representing the degree of supercooling), and $\Delta G'$ denotes the activation energy of molecular motion.

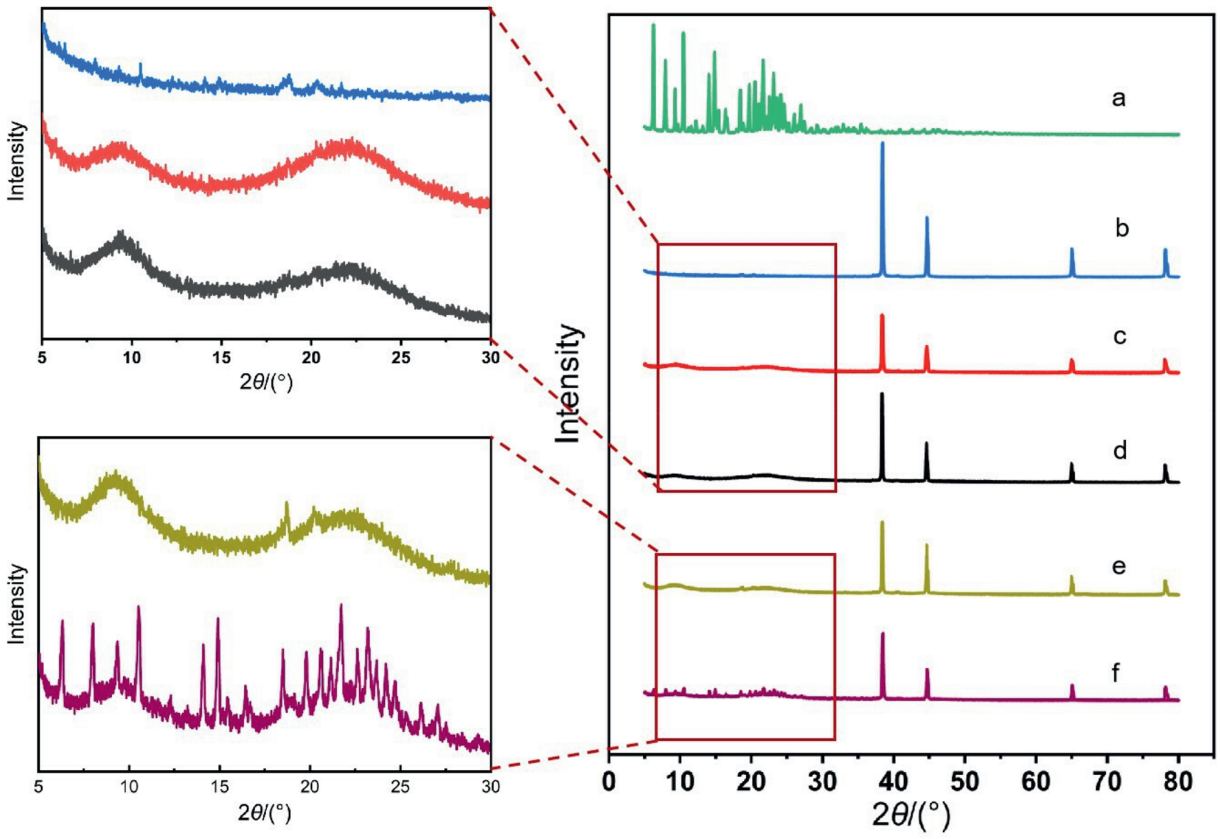

Fig. 9. XRD patterns of various samples: (a) SOA, (b) nano-Al, (c) composite microspheres analyzed after preparation (0 min), (d) composite microspheres analyzed 40 min after preparation, (e) composite microspheres stored at 4 °C for 1 month, (f) composite microspheres stored at room temperature (25 °C) for 1 month. The right panel displays the full 2θ range, while the two panels on the left present expanded views of the 5°–30° 2θ region, providing a detailed comparison of structural changes among the samples.

The mathematical model of crystal growth can be expressed as follows,

$$U = \frac{CT\omega}{\eta}\left[1 - \exp\left(-\frac{\Delta G_V}{kT}\right)\right] \quad (5)$$

where U represents the crystal growth rate, C denotes a constant, T is the measured temperature, ω is a constant related to the growth mechanism, η represents the viscosity of the system, ΔG_V represents the free energy difference between the amorphous form and the crystalline state, and k represents the Boltzmann constant.

In summary, at room temperature (25 °C), the system provides sufficient nucleation driving force and molecular mobility to promote the transition from the amorphous to crystalline state. In contrast, storage at 4 °C significantly suppresses molecular thermal motion and diffusion capabilities, maintaining the amorphous structure in a metastable state. This conclusion not only clarifies the kinetic mechanisms underlying structural evolution in composite microspheres during storage but also provides insights for controlling the physical stability of energetic materials under long-term storage. By optimizing storage temperatures (*e.g.*, below 4 °C), crystal transformation can be effectively inhibited, ensuring reliable material performance.

4. Conclusions

This study successfully developed SOA/Al composite microspheres *via* melt spray technology. The effects of process parameters such as atomizing gas pressure and temperature, as well as polymer additives, were systematically explored to optimize the particle size, morphology, and stability of the microspheres. Composite microspheres with a D_{50} of 35.09 μm were successfully prepared at 150 °C and 200 kPa atomizing gas pressure. The incorporation of 2.5% (mass) PEG:PVP (1:1) blend enhanced microsphere circularity (0.85) and produced a smooth surface with uniform morphology. The XRD and DSC analyses confirmed that the rapid solidification *via* melt quenching led to the formation of amorphous microspheres. Additionally, the melt spray technology enabled laboratory-scale production, yielding 78 g of composite microspheres in 20 min, demonstrating its potential for high-throughput manufacturing of energetic composites. Additionally, the study demonstrated that storage conditions played a critical role. Room-temperature storage induced amorphous-to-crystalline transition, whereas storage at 4 °C preserved the amorphous structure. The melt spray technology utilized in this work provides a scalable, efficient, and environmentally friendly approach for the production of energetic materials doped with nano-Al. Specifically, by adjusting ingredient properties to match the model system, along with adopting the process parameters and atomization strategies developed in this study, the preparation of such composite materials can be directly guided. Significantly, this research provides key insights into the controllable fabrication of micro-nano composite materials, especially those with thermally stable nanomaterials like nano-Al.

CRediT Authorship Contribution Statement

Yilin Liu: Writing – review & editing, Writing – original draft, Visualization, Validation, Investigation, Formal analysis, Data curation. Lanqi Zhang: Supervision. Yulong Yin: Supervision. Nan Li: Supervision. Xiangnan Chu: Supervision. Qi Ma: Supervision.

Jing Liu: Investigation. Wenbo Yang: Writing – review & editing, Methodology, Investigation, Funding acquisition, Formal analysis, Conceptualization. Yingdi Lv: Supervision, Funding acquisition. Shengyang Tao: Writing – review & editing, Supervision, Resources, Project administration, Methodology, Funding acquisition, Conceptualization.

Declaration of Competing Interest

The authors declare that they have no known competing financial interests or personal relationships that could have appeared to influence the work reported in this paper.

Acknowledgements

The authors would like to acknowledge the financial support from the National Natural Science Foundation of China (22272017, 22372025), the Excellent Youth Fund of Liaoning Province (2024JH3/10200005), the Fundamental Research Funds for the Central Universities (DUT25Z2722, DUT22LAB607).

Supplementary Material

Supplementary data to this article can be found online at https://doi.org/10.1016/j.cjche.2025.09.014.

References

[1] G.N. Kokila, C. Mallikarjunaswamy, V.L. Ranganatha, A review on synthesis and applications of versatile nanomaterials, *Inorg. Nano Met. Chem.* 54 (10) (2024) 942–971.
[2] X.J. Zhu, C. Vo, M. Taylor, B.R. Smith, Non-spherical micro- and nanoparticles in nanomedicine, *Mater. Horiz.* 6 (6) (2019) 1094–1121.
[3] X. Wang, H.Y. Li, C. Chen, Z.H. Liang, Understanding of endo/lysosomal escape of nanomaterials in biomedical application, *Smart Mol.* (2025) e20240017.
[4] X.H. Cao, C.L. Tan, M. Sindoro, H. Zhang, Hybrid micro-/nano-structures derived from metal–organic frameworks: preparation and applications in energy storage and conversion, *Chem. Soc. Rev.* 46 (10) (2017) 2660–2677.
[5] Y.F. Si, Z.G. Guo, Superhydrophobic nanocoatings: from materials to fabrications and to applications, *Nanoscale* 7 (14) (2015) 5922–5946.
[6] C. Zhang, D.J. Wu, L.M. Shi, Y.P. Zhu, D.Y. Xiong, S.H. Xu, R. Huang, R.J. Qi, W.C. Zhang, L.W. Wang, P.K. Chu, Manganese molybdate nanoflakes on silicon microchannel plates as novel nano energetic material, *R. Soc. Open Sci.* 4 (12) (2017) 171229.
[7] N.M. Song, L. Yang, J.M. Han, J.C. Liu, G.Y. Zhang, H.X. Gao, Catalytic study on thermal decomposition of Cu-en/(AP, CL-20, RDX and HMX) composite microspheres prepared by spray drying, *New J. Chem.* 42 (23) (2018) 19062–19069.
[8] H.H. Zhou, R. Pujales-Paradela, P. Groppe, S. Wintzheimer, K. Mandel, Tuning the morphology of spray-dried supraparticles: effects of building block size and concentration, *Part. Part. Syst. Char.* 39 (11) (2022) 2200127.
[9] W.Y. Wu, W.J. Liu, X.J. Fu, L. Xu, D.Q. Fan, X.D. Li, S.Q. Hu, Construction of HMX/FOX-7 composite microspheres with controlled microstructures using continuous self-assembly spray drying: to improve safety and combustion performance, *Mater. Chem. Phys.* 339 (2025) 130795.
[10] K. Zhao, J. Zhao, C.J. Wu, S.W. Zhang, Z.W. Deng, X.X. Hu, M.L. Chen, B. Peng, Fabrication of silver-decorated sulfonated polystyrene microspheres for surface-enhanced Raman scattering and antibacterial applications, *RSC Adv.* 5 (85) (2015) 69543–69554.
[11] H. Yabu, Fabrication of nanostructured composite microspheres based on the self-assembly of polymers and functional nanomaterials, *Part. Part. Syst. Char.* 36 (9) (2019) 1900178.
[12] H.X. Liu, C.B. Zhou, X.Y. Liu, Y. Xu, S.M. Geng, Y.H. Chen, C. Wei, C.B. Yu, PMMA@SCNC composite microspheres prepared from Pickering emulsion template as curcumin delivery carriers, *J. Appl. Polym. Sci.* 135 (15) (2018) 46127.
[13] Y. Gong, Q.L. Liu, A.M. Zhu, Q.G. Zhang, One-pot synthesis of poly(*N*-isopropylacrylamide)/chitosan composite microspheres *via* microemulsion, *Carbohydr. Polym.* 90 (1) (2012) 690–695.
[14] S.Y. Kashani, A. Afzalian, F. Shirinichi, M. Keshavarz Moraveji, Microfluidics for core–shell drug carrier particles–a review, *RSC Adv.* 11 (1) (2021) 229–249.
[15] W.B. Zuo, N. Li, Y. Zhao, T.T. Fu, W.L. Fei, R. Yu, J.H. Yang, Synchronized release of bufadienolides in a stable Lutrol F127 based solid dispersion prepared with spray congealing, *Drug Dev. Ind. Pharm.* 44 (11) (2018) 1817–1825.
[16] W.J. Liu, F.Z. Cai, X.D. Li, P.L. Kang, Q.C. Jiang, J.B. Guo, Spherical preparation and performance analysis of FOX-7/RDX energetic composite particles, *Mater. Today Commun.* 47 (2025) 113180.
[17] C. Engelmann, U. Kragl, Spray congealing as innovative technique for enzyme encapsulation, *J. Chem. Technol. Biotechnol.* 93 (1) (2018) 191–197.
[18] S. Bertoni, B. Albertini, N. Passerini, Spray congealing: an emerging technology to prepare solid dispersions with enhanced oral bioavailability of poorly water soluble drugs, *Molecules* 24 (19) (2019) 3471.
[19] H. Tang, Y.T. Wang, W.J. Zhang, L. Shen, Y.B. Duan, J. Hu, Influence of heat treatment on lithium orthosilicate pebbles, *Adv. Mater. Res.* 624 (2012) 208–211.
[20] Z.P. Cheng, X.Z. Chu, W. Zhao, J.Z. Yin, B.L. Dai, H. Zhong, J.M. Xu, Y. Jiang, Controllable synthesis of Cu/Al energetic nanocomposites with excellent heat release and combustion performance, *Appl. Surf. Sci.* 513 (2020) 145704.
[21] S.J. Wang, D. Wang, P. Chen, S. Yan, Q.J. Jiao, X.Y. Guo, Preparation and characterization of Al@TKX-50@NC composite microspheres by electrospray, *Mater. Chem. Phys.* 305 (2023) 127910.
[22] M. Yang, D.Z. Gao, T. Wen, J. Guo, X.Q. Zhang, Q. Wang, C.P. Guo, Efficient construction of Al/F microspheres in Pickering emulsion to regulate combustion reactivity, *J. Mater. Sci.* 59 (7) (2024) 2828–2840.
[23] M.H. Li, A.M. Pang, W. Li, Y.Y. Zhang, X.W. Lv, Z.Y. Ma, Combustion performances of spherical Al/AP nanoenergetic composites produced by solvent evaporation and crystallization, *Combust. Sci. Technol.* 194 (4) (2022) 801–814.
[24] W.Q. Pang, X.Z. Fan, K. Wang, Y.M. Chao, H.X. Xu, Z. Qin, F.Q. Zhao, Al-based nano-sized composite energetic materials (nano-CEMs): preparation, characterization, and performance, *Nanomaterials* 10 (6) (2020) 1039.
[25] J.Q. Jing, X.Y. Zhang, L. Gao, F.B. Gao, H.B. Huo, S.C. Shi, W.J. Cheng, C.H. Xu, J. Y. Wang, C.W. An, Continuous preparation of multi-scale HMX-based energetic composite microspheres by pipe-stream technology, *Powder Technol.* 426 (2023) 118640.
[26] X.Y. Zhang, J.Q. Jing, J.Y. Liu, L.T. Zhang, L.X. Qi, C.W. An, Continuous pipe-stream self-assembly technology for preparation of high sphericity FOX-7/HMX energetic composite microspheres, *APL Mater.* 12 (5) (2024) 051111.
[27] F.Y. Chen, C.L. Xuan, Q.Q. Lu, L. Xiao, J.Q. Yang, Y.B. Hu, G.P. Zhang, Y.L. Wang, F.Q. Zhao, G.Z. Hao, W. Jiang, A review on the high energy oxidizer ammonium dinitramide: its synthesis, thermal decomposition, hygroscopicity, and application in energetic materials, *Def. Technol.* 19 (2023) 163–195.
[28] B. Liu, Y.F. Yang, J. Dong, J.P. Zhang, Design of mineral oil/stearic acid hybrid coatings for reducing hygroscopicity of ammonium nitrate, *Langmuir* 40 (31) (2024) 16653–16661.
[29] J.H. Yu, Y. Kou, L. Xiao, Q.Q. Lu, X.R. Xu, J.Q. Yang, W. Jiang, G.Z. Hao, Efficient construction of core/double-shelled structured AP@nano-graphite@F(2603) energetic microcapsules with low sensitivity and hygroscopicity, *Nanoscale* 17 (5) (2025) 2769–2781.
[30] W.C. Stagner, S. Gaddam, R. Parmar, A.K. Ghanta, Sucrose octaacetate, in: Profiles of Drug Substances, Excipients and Related Methodology, vol. 44, Academic Press, Amsterdam, 267–291 (2019).
[31] E.L. Dreizin, Metal-based reactive nanomaterials, *Prog. Energy Combust. Sci.* 35 (2) (2009) 141–167.
[32] G.K. Batchelor, An Introduction to Fluid Dynamics, Cambridge University Press, Cambridge (2000).
[33] C.Y. Yu, B.H. Wang, X.Z. Wang, Spray Drying Technology, Chemical Industry Press, Beijing (2013). (in Chinese)
[34] R.P.F.N. Dombrowski, A photographic investigation into the disintegration of liquid sheets, *Philos. Trans. R. Soc. Lond. Ser. A Math, Phys. Sci.* 247 (924) (1954) 101–130.
[35] R. Thakkar, R. Thakkar, A. Pillai, E.A. Ashour, M.A. Repka, Systematic screening of pharmaceutical polymers for hot melt extrusion processing: a comprehensive review, *Int. J. Pharm.* 576 (2020) 118989.
[36] P.G. Debenedetti, F.H. Stillinger, Supercooled liquids and the glass transition, *Nature* 410 (6825) (2001) 259–267.
[37] C. Bhugra, M.J. Pikal, Role of thermodynamic, molecular, and kinetic factors in crystallization from the amorphous state, *J. Pharm. Sci.* 97 (4) (2008) 1329–1349.
[38] I.S. Gutzow, J.W.P. Schmelzer, The Vitreous State: Thermodynamics, Structure, Rheology, and Crystallization, Springer, Berlin (2013).
[39] J.J. Zhang, S. Qian, Y. Gao, Theory and Practice of Polymorphic Drug Development, Chemical Industry Press, Beijing (2019). (in Chinese)